Construction and Building Materials 306 (2021) 124914

Contents lists available at ScienceDirect

Construction and Building Materials

journal homepage: www.elsevier.com/locate/conbuildmat

Corrosion resistance of ultra-high performance fibre- reinforced concrete

M. Valcuende [a,*], J.R. Lliso-Ferrando [a,b], J.E. Ramón-Zamora [c], J. Soto [b]

[a] Department of Architectural Constructions, Universitat Politècnica de València, Camino de vera s/n, Valencia 46022, Spain
[b] Research Institute for Molecular Recognition and Technological Development (IDM), Universitat Politècnica de València, Camino de Vera, s/n., Valencia 46022, Spain
[c] Consejo Superior de Investigaciones Científicas, Instituto Eduardo Torroja de Ciencias de la Construcción (CSIC-IETcc), c/Serrano Galvache, 4, Madrid 28033, Spain

ARTICLE INFO

Keywords:
Ultra-high performance fibre-reinforced concrete
Carbonation
Chlorides
Resistivity
Corrosion rate

ABSTRACT

The corrosion resistance of ultra-high performance concrete (UH) made with different fibre contents and under distinct curing conditions was studied. No signs of carbonation were observed after 1 year of accelerated carbonation testing (3% CO_2). The fibreless UHs' electrical resistivity was above 5000 Ω·m, although these values were 2-fold higher than a UH with 1% fibres and approximately 5-fold higher than a UH with 2% fibres. Concrete resistance to chloride penetration was also extremely high (the diffusion coefficient equalled $1.3{\cdot}10^{-13}$ m^2/s) and curing temperatures of 60 °C or 90 °C improved even more these properties, while lack of curing made them slightly worse. Given these excellent properties, the corrosion rate in specimens submerged in chloride solution for 1 year was negligible (i_{CORR} from 0.007 to 0.025 μA/cm^2). These values remained stable with time, unlike the 50 MPa concrete at 2 months when i_{CORR} starting to increase and was 12-fold higher after 1 year. The time estimated for corrosion onset in UH is on average about 150-fold higher than that of 50 MPa.

1. Introduction

One of the most frequent causes of damage in reinforced concrete structures of very high economic importance is rebar corrosion. Several studies point out that corrosion is the dominant degradation mechanism in 70–90% of structures presenting premature deterioration [1]. Fundamentally, two basic mechanisms of destruction of the passive oxide layer protecting rebars are carbonation and the action of chloride ions. In both cases, one of the most influential factors for corrosion process kinetics and, thus, for the durability of reinforced concrete structures, is the material's permeability. Using more waterproof and gasproof concrete prolongs the service life of structures and reduces maintenance costs, which means more sustainable constructions. One good solution for very important structures or for those located in very aggressive environments is to use ultra-high performance concrete (UHPC). This concrete type started being developed in the 1990s [2,3], and is characterised by having excellent mechanical properties and high durability thanks to a very dense porous structure [4,5]. It is manufactured with w/b ratios below 0.2, without coarse aggregates and with large amounts of cement and additions, especially silica fume. Steel fibres also tend to be included in mixes to control cracking by shrinkage, improve mechanical properties and increase concrete ductility. Its compressive strength tends to exceed 150 MPa, although some standards, such as the Swiss SIA 2052:2016 or the American ASTM C1856, set a threshold of 120 MPa.

Most studies about this material have focused on analysing its microstructure and mechanical properties. There are some research works on corrosion, but they offer unalike results because very different UHPCs were used in the tests. In fact the range of strengths worked on is very wide, from 120 MPa to more than 250 MPa, which make comparing the material's performance a hard task. This means that some authors have not detected any signs of carbonation in UHPCs [6–8], while others state that carbonation depth is approximately 2.5- and 4.5-fold lower than that of high-performance concrete C100 and ordinary concrete C35, respectively, after 3 years [9]. Pierard et al. [10] reported a certain degree of carbonation after 1-year exposure to a 1% CO_2 atmosphere. On resistance to chloride penetration, all the authors coincide in UHPCs' excellent performance, and such penetration is practically negligible in specimens submerged in chloride solution [11–14]. Yet, once again, some authors' results differ from those of others. Roux et al. [6] performed diffusion tests in concretes of 230 MPa, but did not obtain any conclusive results because they obtained a chloride concentration with their concrete that went below the sensitivity threshold limit for the experimental method that they followed. During chloride migration

* Corresponding author.
E-mail addresses: mvalcuen@csa.upv.es (M. Valcuende), jollife2@alumni.upv.es (J.R. Lliso-Ferrando), jose.ramon@ietcc.csic.es (J.E. Ramón-Zamora), juansoto@qim.upv.es (J. Soto).

https://doi.org/10.1016/j.conbuildmat.2021.124914
Received 5 March 2021; Received in revised form 23 July 2021; Accepted 11 September 2021
Available online 22 September 2021

testing in the steady state, the same authors obtained a diffusion coefficient in the order of 10^{-14} m^2/s, which was 30-fold lower than in concrete of 90 MPa, and was 55-fold lower than conventional concrete of 35 MPa. Tafraoui et al. [7] reported similar coefficients, but in much less strength concretes, namely 155 MPa. In non-steady state tests, the diffusion coefficient values recorded by Song et al. [15] in concretes of 115–140 MPa were clearly higher by a mean of $4{\cdot}10^{-12}$ m^2/s. Nonetheless, these results differed by approximately one order of magnitude from this obtained by Piérard et al. [10] in concretes of 130–160 MPa, and by about two orders of magnitude from those of Sohail et al. [8] in concretes with similar strength. Nor does the influence of steel fibre content on chloride permeability come over clearly because some authors indicate that it had no impact [16], while others state that it tends to rise with increasing volume [15] and others, conversely, point out less permeability when higher fibre content is used [17,18].

Based on the premises listed above, the objective of the present experimental work was to study the corrosion resistance of UHPC. To this end, a reference UHPC was designed whose compressive strength lay at the lower threshold, which is normally considered for these concretes; that is, from 120 to 150 MPa, and in such a way that its properties would correspond approximately to the minimum ones expected for this concrete type. The effect of a number of parameters, such as steel fibre content or curing conditions, was analysed by comparing the results to values observed in high-strength concrete. Fibre content was limited to a maximum 2% in volume because, as pointed out by Song et al. [15], higher fibre contents do not significantly improve mechanical UHPC properties, and may affect durability. The present work analysed the resistance of UHPCs to the two main factors that trigger corrosion: carbonation and chloride ions. It also studied the material's electrical resistivity because corrosion process kinetics depends on this parameter. It also included a 1-year follow-up of the corrosion rate in specimens submerged in chloride solution.

2. Experimental programme

2.1. Concrete mixtures and materials

Six ultra-high performance concretes (UH) were produced with three distinct fibre contents (0%, 1%, 2%) and four different curing conditions (laboratory environment, climate chamber at 20 °C, 60 °C, 90 °C). UHs were designed in such a way that the compressive strength of the fibreless concrete cured at 20 °C was the minimum one normally considered for this concrete type, i.e. between 120 and 150 MPa. A high-strength concrete 50 MPa (C50) was also made and cured for 28 days in a climate chamber at 20 °C and 95% RH. Three batches were made from each mix.

As regards the UHs curing conditions, the process followed was as follows:

- UH cured in laboratory environment: specimens were air-dried in a laboratory environment to simulate lack of curing.
- UH cured at 20 °C: specimens were left at 20 °C and 95% RH for 28 days.
- UH cured at 60 °C or 90 °C: specimens were left at these temperatures for 48 h and at 100% RH, and were later cured at 20 °C and 95% RH until the age of 28 days.

To produce the UHs, CEM I 42,5 R/SR cement was used, as was silica fume with more than 90% silica content. Two types of silica sand were employed as aggregates: a fine 0/0.5 one and a medium 0.6/1.2 one, along with silica flour of a similar particle size distribution to that of cement. The employed additive was Sika ViscoCrete 20 HE, and its dose was adjusted to obtain similar fluidity characteristics to self-compacting concrete. Steel fibres were employed (13 mm long, 0.2 mm diameter) with almost all the UHs. The nomenclature utilised to identify these concretes refers to the percentage of fibres in the mix (0F, 1F, 2F) and to curing conditions (air, 20 °C, 60 °C or 90 °C).

In concrete C50, the same type of cement was used, but in different quantities. The employed aggregates were 0/4 sand and 4/7 gravel. Table 1 shows the characteristics of each mix and their compressive strength.

2.2. Test methods

In order to analyse concretes' corrosion resistance, tests were done to determine the corrosion rate and resistance to the penetration of aggressive substances that can depassivate steel (accelerated carbonation test, chloride migration test and chloride diffusion test). The electrical resistance test was also carried out as this parameter is related to the corrosion rate (the corrosion process only happens if the current, transported by ions in the pore solution, can circulate inside the concrete between the anodic and cathodic areas of the reinforcement).

In addition, the compressive strength at the ages of 28 and 365 days was determined from each mix on cylindrical specimens 100 mm in diameter and 200 mm high (Table 1).

a) Accelerated carbonation test

This test was carried out in accordance with Standard UNE 83993-2:2013. For this purpose, prismatic specimens (40x40x160 mm) were made. Before tests started, specimens were dried at 50 °C and leaving them for 21 days in a chamber at 20 °C and 70% RH. After this time, the specimens were placed inside a curing chamber with 3% CO_2 at 20 °C and 65% RH, and were left under these conditions for 378 days. Different research works coincide when pointing out that accelerated carbonation testing performed at the 3% CO_2 concentration produces similar carbonation to that obtained in the long term under natural carbonation conditions [19].

Carbonation was followed up one a week for the first 1.5 months, and every 2 weeks thereafter. Three batches were made with each concrete type, and two specimens were produced per batch. The arithmetic mean of the six obtained values was taken as each test result.

b) Chloride migration test

This test provides a measure of concrete resistance to chloride penetration. It was performed in accordance with Standard NT BUILD 492. Cylindrical specimens were used (100 mm diameter, 50 mm high). At the testing age, they were vacuum-saturated with calcium hydroxide. They were placed by allowing one side to come into contact with a 2-molar chloride solution, and the other side with a 0.3-molar sodium hydroxide solution. Then a potential differential was applied between both specimen sides to force chloride migration through concrete. When testing ended, specimens were axially split and the cover was sprayed with silver nitrate solution. The chloride-polluted areas became whitish. This enabled the penetration depth to be measured and the chloride migration coefficient was determined according to the expression set out in the standard.

Testing was done at two ages: 28 and 365 days. Three batches were made with each concrete type, and two specimens were produced per batch. The arithmetic mean of the six obtained values was taken as each test result.

c) Chloride diffusion test

Chloride penetration to the concrete interior takes place mainly by diffusion. To perform these tests, cylindrical specimens were used (100 mm diameter, 100 mm high), which were cured for 28 days. A water tank with 0.5 M chloride was placed on one of the specimen sides and epoxy coating was applied to the others (Fig. 1). Given the low UH permeability, the water tank was 500 mm high and specimens were left under these conditions for 1 year. After this time, the chloride

Table 1
Mixture proportions of concrete (kg/m^3) and compressive strength (MPa).

	UH-0F-20	UH-1F-20	UH-2F-20	UH-2F-air	UH-2F-60	UH-2F-90	C50
Cement	800	800	800	800	800	800	450
Water	160	160	160	160	160	160	225
Superplastificiser	30	30	30	30	30	30	1.37
Silica fume	175	175	175	175	175	175	—
Silica flour	225	225	225	225	225	225	—
Sand (0/0.5)	302	302	302	302	302	302	—
Sand (0.6/1.2)	565	565	565	565	565	565	—
Sand (0/4)	—	—	—	—	—	—	880
Gravel (4/7)	—	—	—	—	—	—	880
Steel fibres	160	80	160	160	160	160	—
w/b [(*)]	0.19	0.19	0.19	0.19	0.19	0.19	0.50
f_c (28 days)	129.8	129.9	128.4	137.9	145.7	154.2	49.9
f_c (365 days)	152.1	149.0	163.4	157.0	161.3	166.3	56.3

[(*)] includes the aqueous part of the SP.

Fig. 1. Water tank with chlorides placed on the specimens.

concentration was measured at different depths. To do so, the specimen was cut into 5 mm-thick perpendicular slices to the water flow direction, and chloride content was determined in them all in line with Standard NT BUILD 208. Three batches were made with each concrete type, and two specimens were produced per batch. The arithmetic mean of the six obtained values was taken as the test result.

d) Electrical resistance test

Tests were run in prismatic specimens (40×40×160 mm) according to Spanish standard UNE 83988-1:2008. Electrical resistance was determined by the direct method by applying a uniform electric field using two flat stainless steel electrodes (40x40 mm) that came into contact with the specimen bases. The two specimens ends were cut to remove the concrete layer cover in the area where electrodes were placed. This was performed because this layer was richer in cement than the rest of the specimen owing to the wall effect that occurs during casting in the areas that come into contact with formworks. Tests were performed with the specimens under a saturated surface dry condition because the degree of concrete saturation affects their electrical resistance.

Measurements were taken with a commercial conductivity meter (Portavo 904). The inverse of conductance is the material's electrical resistance. To ensure good electrical contact between electrodes and specimen, some previously dampened sponges with the same area that electrodes had were placed. Moreover, in order to ensure that the applied pressure was homogeneous, a press with two nylon plates and metal bars was used (Fig. 2). The value was recorded 5 min after measurements commenced to ensure that the recorded signal was stable enough. Measurements were taken at different ages 3 months after producing samples.

Three specimens were made with each concrete type, and the arithmetic mean of the three obtained values was taken as each test result.

e) Corrosion rate test

Tests were carried out in cylindrical specimens (50 mm diameter, 100 mm height) with a bar (10 mm diameter, 100 mm long) inserted into the centre. The concrete cover of the bar was 20 mm. The two bar ends were protected with epoxy resin, and the steel area that came into contact with concrete measured 18.42 cm^2. The electrical contact for

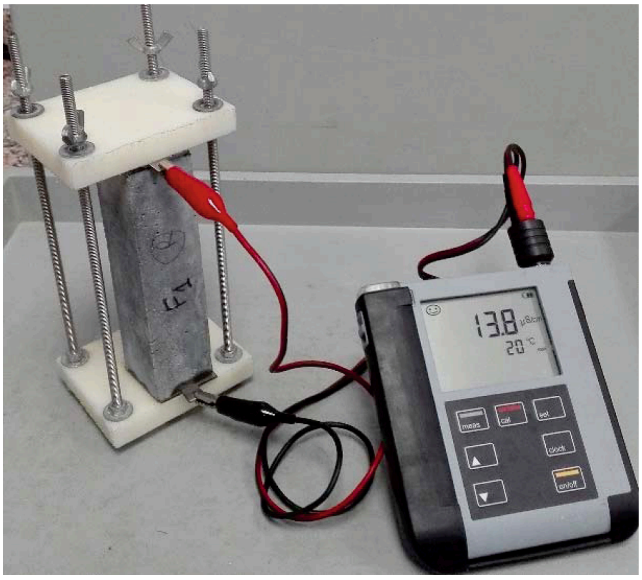

Fig. 2. Measuring conductance in prismatic specimens.

measurements was at the end of the bar, which was protected with Vaseline in order to prevent corrosion. After 28 days, specimens were partly submerged (up to mid-height) in 0.5 M sodium chloride solution and were left under these conditions for 1 year.

The corrosion current is the rate at which anodic or cathodic reactions occur on rebars, and the corrosion current density (i_{CORR}) is the current per unit area of the rebar. To calculate i_{CORR}, the Potentiostatic Step Voltammetry method described in [20] was followed. This method is based on the Tafel extrapolation method, but a symmetrical potentiostatic pulse pattern of various amplitudes was applied to obtain the linear stretches of the anodic and cathodic Tafel curves. The i_{CORR} value is established from the intersection of both lines, considering the ohmic drop between the bar and concrete surface. Using pulses instead of long and slow linear sweep voltammetry allows corrosion density to be very quickly measured and avoids polarising rebar. Having determined i_{CORR}, the following equation, which derives from Faraday's law, can be used to calculate the corrosion rate:

$$v_{CORR} = 3.27 \cdot \frac{i_{CORR} \cdot M}{\rho . n} = 11.6 \cdot i_{CORR} \quad (1)$$

where v_{CORR} is the corrosion rate (μm/year), i_{CORR} is corrosion current density (μA/cm^2), M is the atomic mass of steel (g/mole), ρ is steel density (g/cm^3) and n is the number of electrons in the reaction (2 with iron).

The corrosion current density measurements were taken using a three-electrode cell, where the embedded rebar was the working electrode. The employed reference electrode was a saturated calomel electrode, and a stainless steel mesh acted as the counter electrode, which was placed around the specimen to make the electric field as homogeneous as possible (Fig. 3). A wet cloth was placed between the concrete surface and the counter electrode to ensure good electrical contact. An Autolab PGSTAT 100 potentiostat was employed for measurements. To reduce electrical noise, tests were run in a Faraday cage. Six specimens were made per concrete and the arithmetic mean of the six obtained values was taken as the test result.

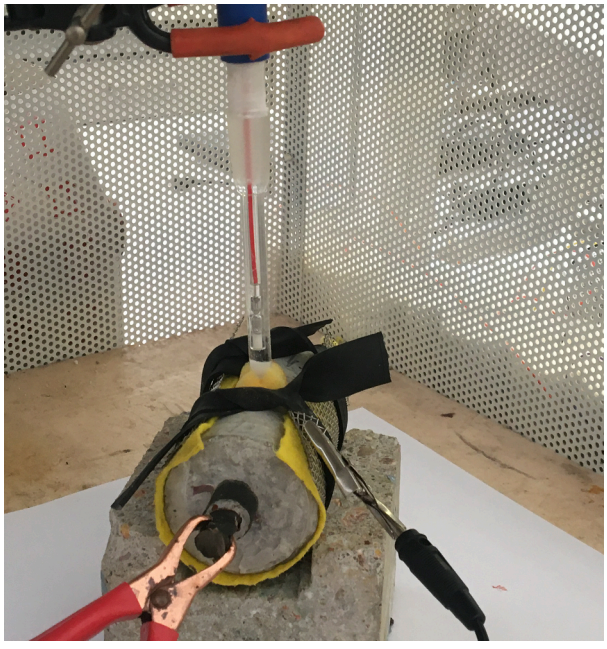

Fig. 3. Setup for the electrochemical measurements.

3. Results and discussion

3.1. Carbonation resistance

When calcium hydroxide is combined with CO_2, calcium carbonate forms by the following reaction:

$$Ca(OH)_2 + CO_2 \rightarrow CaCO_3 + H_2O$$

As the molecular weight of $Ca(OH)_2$ is 74.10 g/mol and that of $CaCO_3$ is 100.09 g/mol, weight increases during the reaction, and a quantity of water evaporates. By bearing this scenario in mind, and to perform long-term follow-up without having to break specimens, carbonation was controlled by regularly weighing specimens and only occasionally checking carbonation depth by the phenolphthalein method. This procedure also allows the instant when the specimen is completely carbonated to be accurately estimated. In any case, the relation between increased weight and carbonation depth was periodically verified with some specimens. As seen in Fig. 4, the correlation between both parameters was very high, and the R^2 correlation coefficient equalled 0.998.

a) UH versus C50

Fig. 5 represents the weight evolution of the specimens left in the carbonation chamber. It shows a large difference between the UH concretes and the reference concrete 50 MPa. The total carbonation of the specimens with concrete C50 was achieved at the age of 195 days. This was also checked by periodically breaking some specimens and following the phenolphthalein method (Fig. 6).

In all the UHs, except for the poorly cured concrete (UH-2F-air), carbonation depth was still null after 1 year of testing (378 days) and, therefore, the CO_2 diffusion inside the material could be considered either null or practically null (Fig. 7).

b) Effect of curing conditions and fibre content

For the poorly cure concrete (UH-2F-air), Fig. 8 shows the slight increased specimen weight up to the age of 100 days, from which time values stabilised. This weight increase corresponded to concrete carbonation of around 1 mm deep (Fig. 9), which did not continue to evolve. In other words, due to lack of curing, the upper concrete layer became somewhat more porous and, therefore, carbonated. However, this layer thickness was minimum, and CO_2 no longer penetrates once this depth has been reached. When comparing the weight increase curves of concretes UH-2F-air and C50, it was noteworthy that the carbonation rate in the porous layer of UH-2F-air is considerably slower than in concrete 50 MPa. As a guideline and in a very simplified way, if as Ho and Lewis [21] point out, a 1-week exposure in accelerated test

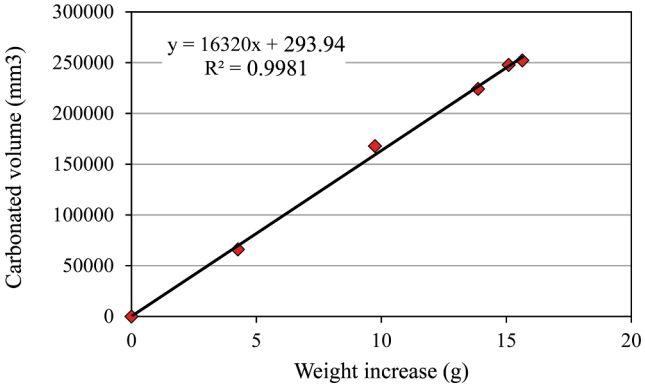

Fig. 4. Relationship between increased specimen weight and carbonated volume.

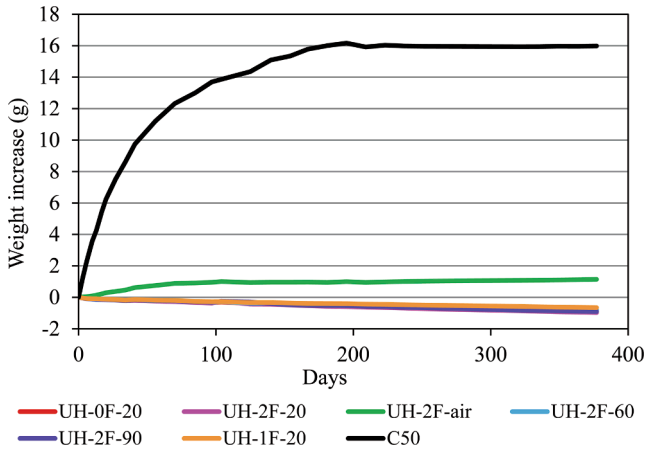

Fig. 5. Weight evolution of the specimens inside the carbonation chamber.

can be considered the equivalent to a 1-year exposure in a normal atmosphere, then the CO_2 diffusion coefficient in the porous layer of UH-2F-air would even be in the order of 13-fold lower than in the high-resistant concrete C50.

For the influence of curing temperature (20 °C, 60 °C or 90 °C) or fibre content (0%, 1%, 2%) on the carbonation of ultra-high-performance concretes, no statistically significant differences were observed between the different concrete types.

In short, according to the obtained results, producing rebar corrosion by the carbonation of UH concretes is not foreseeable because the CO_2 diffusion to the material's interior is null or practically null.

3.2. Resistance to chloride penetration

Chloride penetration which takes place due to migration and diffusion (which are two of the main mechanisms of ions transport inside concrete) was analysed. Migration is due to an electrical potential gradient and diffusion to a concentration gradient.

3.2.1. Chloride migration

Fig. 10 shows the chloride migration D_{nssm} coefficient values in the

Fig. 7. Phenolphthalein method in concrete UH-0F-20 at the age of 1 year.

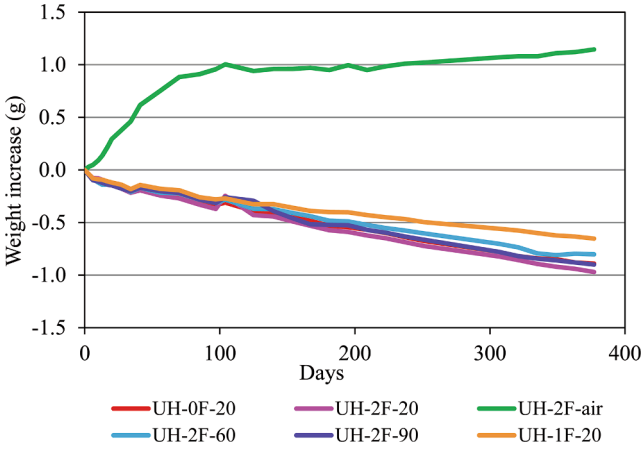

Fig. 8. Specimen weight evolution in UH concretes (accelerated carbonation test).

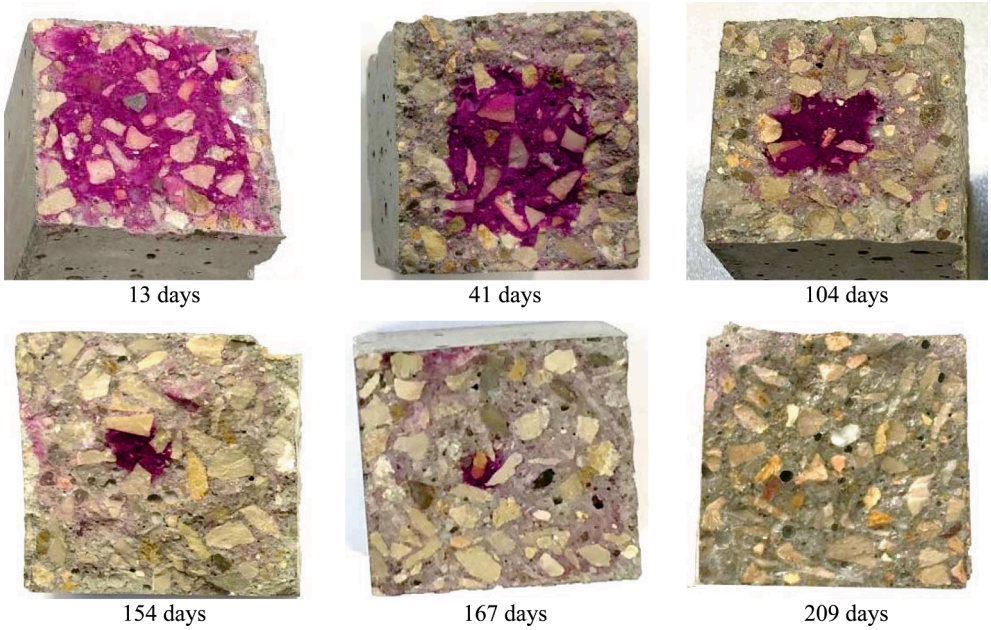

Fig. 6. Carbonation depth of concrete C50 at different ages.

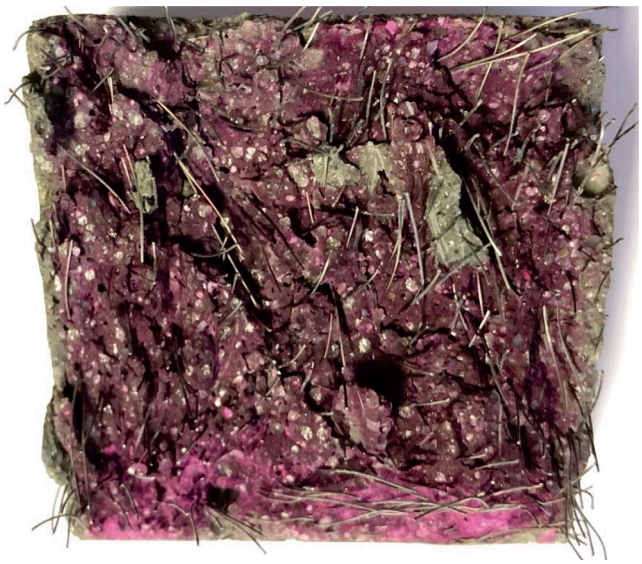

Fig. 9. Carbonation depth of concrete UH-2F-air at the age of 104 days (accelerated carbonation test).

non-steady state. Logically, and in general, the older the age, the lower the D_{nssm} coefficient as a result of the cementitious material's progressive hydration.

a) UH versus C50

The chloride migration that took place in all the UH concretes was much lower than in the reference concrete C50, and the differences between both were around two orders of magnitude. For example, the mean D_{nssm} coefficient value in concretes UH-2F-20 and C50 was $2.0{\cdot}10^{-13}$ m^2/s and $2.1{\cdot}10^{-11}$ m^2/s, respectively, at the age of 28 days. The high UH resistance to chloride penetration is due to two factors. On the one hand, a very dense microstructure, characterised by low porosity, a very fine porous structure and capillary network segmentation, which decrease water permeability (with chlorides dissolved in water). On the other hand, as a result of the high cement content used in UH mixes, the tricalcium aluminate content is also high. This compound easily reacts with chlorides to form calcium chloro-aluminate (Friedel's salt), and therefore the free chlorides content in concrete lower.

b) Effect of curing conditions

When only UHs were analysed, Fig. 10 shows how the initial curing performed at high temperatures (UH-2F-60 and UH-2F-90) increased concrete resistance against chloride penetration at early ages. In fact, the D_{nssm} coefficient for concrete UH-2F-20 at 28 days was, on average, 54% and 82% higher than in UH-2F-60 and UH-2F-90, respectively. According to the porosimetry and SEM results obtained in a previous work [5], this improvement was due to the reduction in the total pore volume and to increased porous structure fineness, which occur with rising curing temperature. Indeed when curing temperature was increased in the first hours, cement hydration accelerated and more portlandite was produced, which pozzolanically reacted with silica fume to, in turn, generate more C-S-H. Moreover, the 90 °C temperature induces higher water vapour pressure, which favours easier and faster vapour penetration through the porous network and, with it, cement hydration and the silica fume pozzolanic reaction. Nevertheless at older ages (365 days), the D_{nssm} coefficient of concretes UH-2F-60 and UH-2F-90 tended to equal that of the UHs cured at 20 °C. At this age, the ANOVA of the results indicated that the differences in the three concretes (UH-2F-20, UH-2F-60 and UH-2F-90) were not statistically significant (p-value = 0.67). That is to say, as with the evolution of compressive strength (Table 1), increased chloride penetration resistance with age was somewhat less in the UHs cured at 60 °C and 90 °C, and their properties tended to equal those of the UH cured at 20 °C in the long-term.

The results in Fig. 10 also show that resistance to chloride penetration was affected by lack of curing. At the two studied ages, chloride penetration depth and, consequently, the D_{nssm} coefficient was in concrete UH-2F-air of the order of the double than in UH-2F-20. Nevertheless, according to the classification by Baroghel-Bouny [22], even with poor curing, the obtained values were indicative of extremely durable concrete (D_{nssm} $<10^{-12}$ m^2/s). Similarly, and based on the criteria provided by [23], UH-2F-air can be classified as having "extremely high" resistance to chloride penetration at 28 days (D_{nssm} $<2.5{\cdot}10^{-12}$ m^2/s).

c) Effect of fibre content

For fibre content (0%, 1%, 2%), the D_{nssm} coefficient in the fibreless concrete (UH-0F-20) and that made with 1% (UH-1F-20) tended to be lower than that produced with 2% (UH-2F-20). However, owing to dispersion of the results, the differences in the three concretes were not statistically significant (p-value equalled 0.07 and 0.24 at 28 and 365 days, respectively). Steel fibres have influenced on the resistance to chloride penetration in two ways, a favourable and an unfavourable one, which tended to counteract one another. On the one hand, they helped to control shrinkage cracking of the cement paste but, on the other hand, they generated weak points through which chlorides more easily penetrated because the interphases among materials are the most porous zones [24,25]. Besides, using higher fibre contents means that fibre balls can form with pores inside them.

3.2.2. *Chloride diffusion*

Fig. 11 represents the total chloride content per weight cement, obtained at the various depths in specimens exposed to sodium chloride

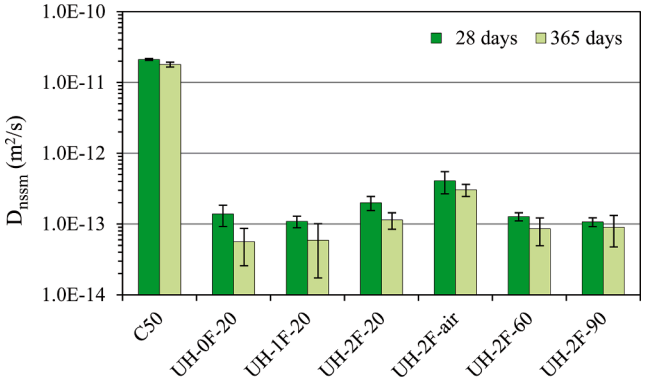

Fig. 10. Chloride migration coefficient.

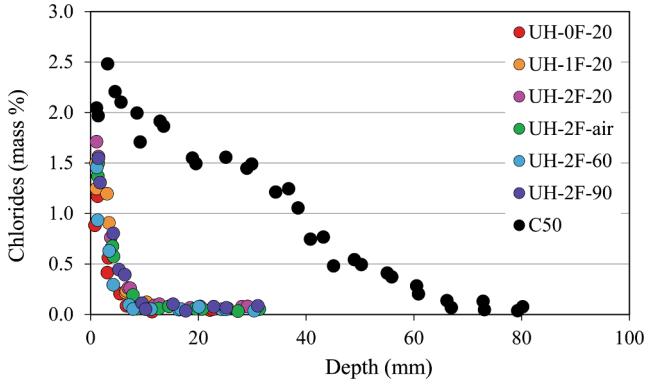

Fig. 11. Chloride penetration profile (content per cement weight).

solution for 1 year.

If, as some authors and certain standards and codes point out [26,27], chloride diffusion inside concrete in the non-steady state can be assumed to approximately follow Fick's second law, the chloride concentration at different depths and at a given age C(x,t) is given by Eq. (2).

$$C(x,t) = C_0 + (C_s - C_0)\left[1 - \mathrm{erf}\left(\frac{x}{2\sqrt{D_{ap}\cdot t}}\right)\right] \quad (2)$$

where the Gaussian error function is:

$$\mathrm{erf}(z) = \frac{2}{\sqrt{\pi}}\int_0^z e^{-u^2}\,du \quad (3)$$

and where C_0 is the initial chloride concentration (chloride content in % mass prior to immersion in NaCl solution), C_s is the chloride concentration on the concrete surface, and D_{ap} is the apparent diffusion coefficient, expressed as m^2/s, that depends on the concrete's characteristics. The initial chloride concentration (chloride contributed by raw materials) per cement weight was experimentally determined in the samples not contaminated by chloride solution, with 0.04% in UH and 0.06% in C50.

The surface chloride concentration (C_s) and the D_{ap} coefficient were obtained by fitting Eq. (2) with the experimental data about the chloride concentration at different depths by a non-linear least squares regression analysis. Fig. 12 represents some of the obtained fit curves and Fig. 13 offers the D_{ap} coefficient results.

a) UH versus C50

The D_{ap} coefficient is a good indirect indicator of durability because it is closely related to concrete resistance to chloride penetration and is, thus, related to the onset of the corrosion period and concrete's service life. The test results were similar to those recorded in the migration tests. Once again, they showed large differences between UH and high-resistance concrete C50, where the D_{ap} coefficient was two orders of magnitude lower than in UH.

In order to evaluate the relevance that these differences have on a structure's service life, the time required for rebar corrosion onset (t_{crit}) was calculated by Eq. (4), which was obtained from Eq. (2):

$$t_{crit} = \frac{x^2}{4\,D_{ap}\left[erf^{-1}\left(\frac{C_s - C_{crit}}{C_s - C_0}\right)\right]^2} \quad (4)$$

where erf^{-1} is the inverse Gaussian error function, x is the concrete cover and C_{crit} is the critical chloride concentration threshold that alters rebar passive layer stability and leads to corrosion onset.

C_{crit} is not a well-defined value in the scientific literature. The higher the chloride concentration on the steel surface, the more likely corrosion onset is. A wide range of values has been suggested [28,29]. By taking

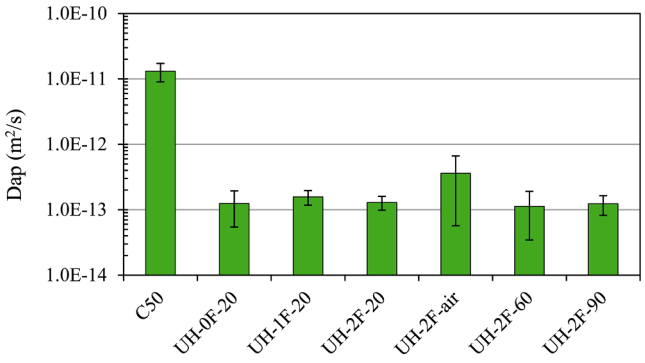

Fig. 13. D_{ap} diffusion coefficients.

1.0% cement weight as a value that some authors suggest [26], Fig. 14 represents the concrete cover-onset corrosion curves. These curves are only estimated and cannot, thus, be taken as a true value, but they allow comparisons to be made between concretes. Once again on them it can be seen large differences between UH and concrete C50. As the calculation shows, the time estimated for corrosion onset in UH is on average about 150-fold higher than that of C50.

b) Effect of curing conditions and fibre content

The D_{ap} coefficient results obtained for UH are similar to those recorded in the migration tests. After a 1-year testing period, neither curing temperature (20 °C, 60 °C or 90 °C) nor fibre content (0%, 1% or 2%) significantly impacted ultra-high performance concrete resistance to chloride diffusion. The mean D_{ap} diffusion coefficient value was approximately $1.3{\cdot}10^{-13}$ m^2/s. Fig. 13 also shows that chloride diffusion was slightly greater with the poorly cured concrete, with a mean D_{ap} value of $3.6{\cdot}10^{-13}$ m^2/s.

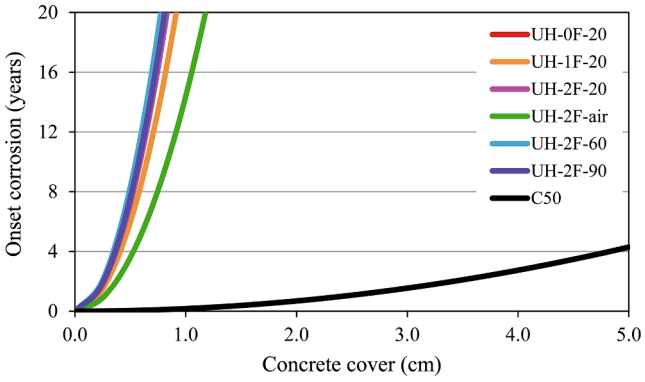

Fig. 14. Rebar corrosion onset (t_{crit}).

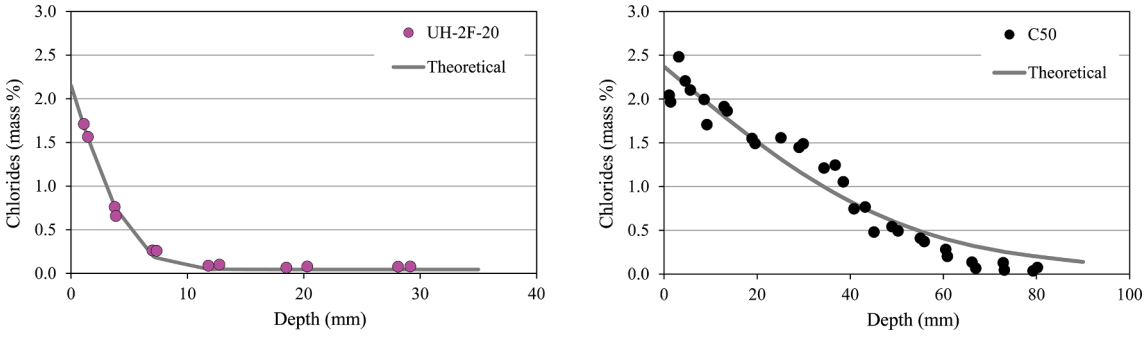

Fig. 12. Experimental values and fit curves in the concrete UH-2F-20 and C50 specimens.

3.3. Electrical resistivity

Electrical resistivity reflects a material's capacity to transport electric charges. Rebar corrosion is an electrochemical process during which, in addition to the electron transport through steel, an ionic current through the dissolved ions in the pore solution must be involved for the electric circuit to close. So by having depassivated rebars, concrete's resistivity controls the corrosion process kinetics. In concrete with high electrical resistivity, the corrosion process is slow because the current cannot easily pass between the anodic and cathodic areas of rebars.

a) UH versus C50

The electrical resistivity (ρ) for each concrete type at different ages is found in Fig. 15. Like all the other analysed properties, a large difference appears in the values recorded in conventional concrete C50 and those for UH, and these differences vary in some cases by more than one order of magnitude. UHs' high resistivity is justified by the material's high compactness, its low porosity and connectivity between pores. In such concretes, ρ values are generally above 1000 Ω·m, which denotes a negligible corrosion risk [30] and very high durability [22].

b) Effect of curing conditions

When only the UH concretes were analysed, Fig. 15 shows that curing temperature initially affected the material's resistivity, although the results obtained in the concretes cured at 60 °C and 90 °C were similar. For example, in UH-2F-20 (cured at 20 °C), the average resistivity value after almost 400 follow-up days was 1100 Ω·m, but concretes UH-2F-60 and UH-2F-90 were 2000 Ω·m and 1900 Ω·m, respectively.

Lack of curing (UH-2F-air) also influenced the ρ values. The mean resistivity in this concrete type was 35% lower than in the concrete cured in a chamber at 20 °C (UH-2F-20), that is, about 700 Ω·cm. According to the results obtained in a previous work [5] and those found by carbonation test, the lower resistivity of concrete UH-2F-air was due to a small more porous concrete surface layer caused by lack of curing.

c) Effect of fibre content

The fibre content (0%, 1%, 2%) results showed that steel fibres increased the material's conductivity as steel possesses negligible resistance to electrons' movement, and the resistivity of the fibreless concrete (UH-0F-20) was around 2-fold and 5-fold greater than the concretes with the 1% and 2% fibre content (UH-1F-20 and UH-2F-20), respectively. That is, fibres act as linkage bridges between pores and, thus, when their content increases they provide the shortcut for the ionic current to flow more easily. In any case, even though fibres significantly reduce concrete resistivity, the resistivity of the UH with 2% fibre content was almost one order of magnitude higher than that of concrete C50.

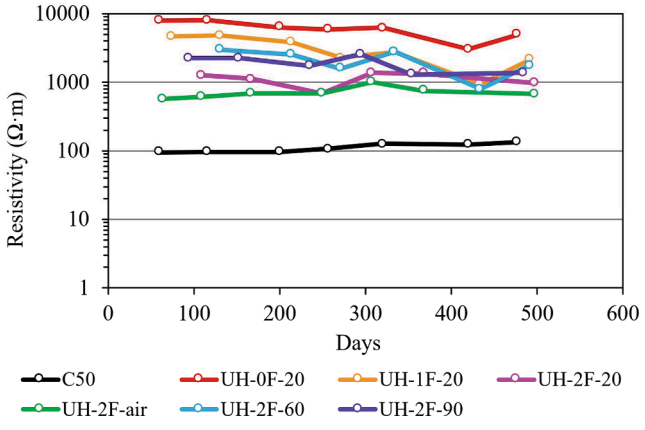

Fig. 15. Resistivity evolution.

3.4. Corrosion rate

Fig. 16 shows the average corrosion density evolution (i_{CORR}) on the semilogarithmic scale of the rebars embedded into specimens partially submerged in chloride solution.

d) UH versus C50

In all cases, e.g., the UH concretes and the conventional concrete, i_{CORR} was not initially negligible, but soon lowered and went below 0.1 μA/cm^2. That is, a low corrosion firstly took place before a protective oxide film was formed on the rebars and then i_{CORR} stabilised. This is because during the first hours after casting, the oxygen content (retained while mixing) and humidity inside the material are high, which favour the rebars corrosion process. Then, during hydration of cement, porosity lowers and pH rises, which allows rebars to passivate and i_{CORR} to decrease. According to some authors, this passive film formation period can take at least 20 days [31], although Fan et al. [32] suggest that UH can take somewhat longer owing to the low oxygen content present in concrete.

In concrete C50, rebar corrosion density tended to increase 2 months after casting; i.e., after specimens were partially submerged in chloride solution for 1 month. This implies that chlorides had started reaching steel and destroying the passive oxide layer. Some researchers state that corrosion onset takes place when the averaged sustained corrosion density is higher than 0.2 μA/cm^2 [27,28,33]. This situation takes place at approximately 1 year. As the concrete cover employed in our tests measured 2 cm, according to the theoretical curves obtained in Section 3.3 (Fig. 14), the estimated time for corrosion onset was slightly more than 8 months and, hence, well agrees with the real obtained data.

The i_{CORR} values in UH were similar in all cases and remained quite stable with time, between 0.007 and 0.025 μA/cm^2 (without considering the values recorded during the first weeks). In other words, accordind to Eq. (1), the corrosion rate (v_{CORR}) lay between 0.08 and 0.29 μm/year, and thus, according to Standards UNE 112072:2011 and ASTM STP 1065, or design guideline RILEM TC-154, these values indicate a negligible corrosion rate ($i_{CORR} \leq 0.1$ μA/cm^2 or $v_{CORR} \leq 1.16$ μm/year). In fact, after 1 year, the i_{CORR} values were around 12-fold lower than those recorded in the high strength concrete C50. This excellent UH corrosion performance was due to their good resistance to chloride penetration (rebars remained in the passive state), high resistivity (current intensity is much lower according to Ohm's law), and also

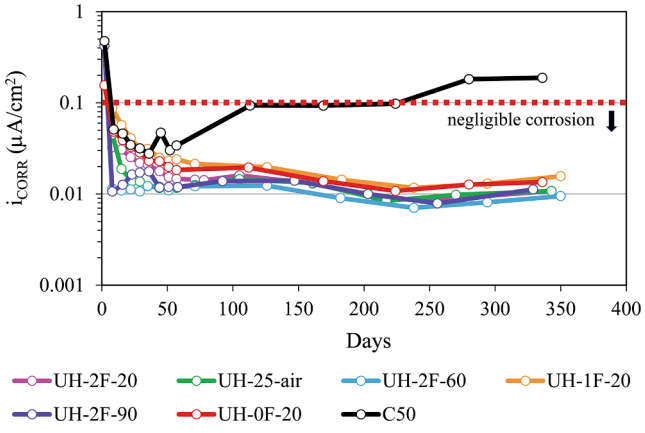

Fig. 16. Corrosion density evolution of specimens submerged in chloride solution.

probably due to a very low oxygen availability.

c) Effect of curing conditions and fibre content

Given negligible rebars corrosion, the obtained i_{CORR} results did not reflect any differences between the concretes submitted to the different curing conditions.

For fibres content, no differences appeared between the different concrete types. Nonetheless in the UH with fibres, small oxide stains were seen due to the oxidation of surface steel fibres. In these concretes, fibres are surrounded by a very dense cementitious paste, which hinders oxide crystal growth and oxygen diffusion [34]. Thus, oxidation affects only the fibres zone closer to the surface (Fig. 17), where there is practically no concrete cover. This minimal corrosion of some surface fibres did not affect resistance to chloride diffusion (see Section 3.2.2.b) and, coherently with this, it did not influence rebar corrosion because the i_{CORR} values in the UHs with fibres (UH-1F-20, UH-2F-20) were the same as those in the fibreless UH (UH-0F-20).

4. Conclusions

The following conclusions can be drawn from the study of the corrosion resistance of the ultra-high performance concretes (UH) made with different fibre volume contents and under distinct curing conditions. UHs were designed to the minimum compressive strength defined for them (120–150 MPa). In this way, the obtained characteristics can be deemed to correspond approximately to the minimum characteristics expected for this concrete type.

- UHs displayed no signs of carbonation after undergoing an accelerated carbonation test for 378 days. Minimum carbonation was detected only in UH-2F-air (1 mm depth) due to a thin more porous concrete surface layer caused by lack of concrete curing. At any rate, this minor carbonation development took place in the first 100 days and then stopped.
- UHs' resistance to chloride penetration can be classified as "extremely high". The migration (D_{nssm}) and diffusion (D_{ap}) coefficients obtained in the non-steady state were $2.0{\cdot}10^{-13}$ m^2/s and $1.3{\cdot}10^{-13}$ m^2/s, respectively. These values were two orders of magnitude lower than those obtained for concrete 50 MPa.
- Initial UH curing at 60 °C or 90 °C increased concretes' resistance to chloride at early ages, and the D_{nssm} coefficient lowered by 54% and 82%, respectively, in relation to one UH cured at 20 °C. Nonetheless, the increase in resistance to chloride penetration with age was somewhat lower in the UHs cured at a higher temperature, and similar D_{nssm} values were obtained for all the UHs at the 1-year age (approximately $1.0{\cdot}10^{-13}$ m^2/s).
- Fibre content (0%, 1% or 2%) did not significantly influence resistance to chloride diffusion in the ultra-high performance concretes.
- Rebar corrosion onset was calculated based on diffusion equations. The results show that the time estimated for corrosion in UHs to start was about 150-fold higher than for concrete 50 MPa.
- Fibreless UHs' electrical resistivity (ρ) was generally above 5,000 Ω·m, although these values may be lower depending on the steel fibre content employing in the mix. The fibreless UHs' resistivity was about 5-fold higher than a UH with 2% fibres, and approximately 2-fold higher than a UH with 1% fibres
- The initial UH curing at 60 °C or 90 °C increased concrete's resistivity in the first months, while lack of curing lowered it. Nonetheless in the long term, the ρ values tended to equal those of a UH cured at 20 °C
- After leaving specimens in chloride solution for 1 year, the corrosion rate of all the analysed UHs was negligible, with i_{CORR} values between 0.007 and 0.025 $\mu A/cm^2$. These values remained stable with time, unlike those observed with concrete 50 MPa because i_{CORR} began to increase after 2 months, and was 12-fold higher after 1 year. UHs' excellent performance was due to their high resistance to chloride penetration and their excellent resistivity.

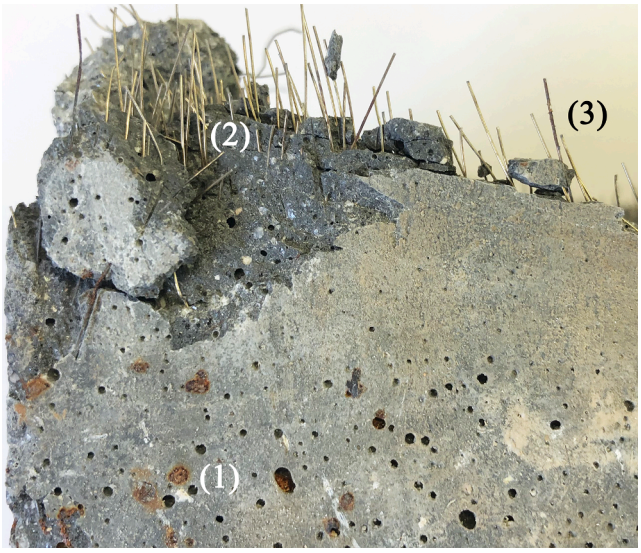

Fig. 17. Concrete UH-2F-20 sample: 1) oxide stains, 2) corrosion-free fibres, 3) fibres with corrosion.

CRediT authorship contribution statement

M. Valcuende: Conceptualization, Methodology, Formal analysis, Writing – original draft, Writing – review & editing, Funding acquisition. **J.R. Lliso-Ferrando:** Investigation. **J.E. Ramón-Zamora:** Software, Investigation. **J. Soto:** Methodology, Funding acquisition, Supervision.

Declaration of Competing Interest

The authors declare that they have no known competing financial interests or personal relationships that could have appeared to influence the work reported in this paper.

Acknowledgements

Authors thank to the Spanish Government the financial support of project BIA2016-78460-C3-3-R and to the European Union's Horizon 2020 the financial support of ReSHEALience project (Grant Agreement No. 760824). Furthermore, authors would like to express their gratitude for the support of the Universitat Politècnica de València. Funding for open access charge: CRUE-Universitat Politècnica de València. The predoctoral scholarship granted to Josep Ramón Lliso Ferrando within the program "Formación de Personal Investigador" from the Universitat Politècnica de València (FPI-UPV-2018) is also gratefully acknowledged.

References

[1] U.E. Angst, Challenges and opportunities in corrosion of steel in concrete, Materials and Structures 51 (2018) 4, https://doi.org/10.1617/s11527-017-1131-6.
[2] P. Richard, M. Cheyrezy, Reactive powder concrete with high ductility and 200–800 MPa compressive strength, in: ACI Spring Convention, SP-144, San Francisco, 1994, pp. 507–508.
[3] F. de Larrard, T. Sedran, Optimization of ultra-high-performance concrete by the use of a packing model, Cem. Concr. Res. 24 (6) (1994) 997–1009, https://doi.org/10.1016/0008-8846(94)90022-1.
[4] J.C. Scheydt, H.S. Muller. Microstructure of ultra high performance concrete (UHPC) and its impact on durability, in: Proceedings of the 3rd International Symposium on UHPC and Nanotechnology for High Performance Construction Materials, Kassel, Germany. 2012. 349e356.
[5] M. Valcuende, J.R. Lliso-Ferrando, J.M. Gandía-Romero, M. Roig-Flores, Porous structure of Ultra-High Performance Fibre-Reinforced Concretes, Materials 14 (2021) 1637, https://doi.org/10.3390/ma14071637.

[6] N. Roux, C. Andrade, M.A. Sanjuan, Experimental study of durability of reactive powder concretes, J. Mater. Civ. Eng. 8 (1) (1996) 1–6.
[7] A. Tafraoui, G. Escadeillas, T. Vidal, Durability of ultra high performances concrete containing metakaolin, Constr. Build. Mater. 112 (2016) 980–987, https://doi.org/10.1016/j.conbuildmat.2016.02.169.
[8] M.G. Sohail, R. Kahraman, N. Al Nuaimi, B. Gencturk, W. Alnahhal, Durability characteristics of high and ultra-high performance concretes, Journal of Building Engineering 33 (2021) 101669, https://doi.org/10.1016/j.jobe.2020.101669.
[9] M. Schmidt, E. Fehling. Ultra-high-performance concrete: research, development and application in Europe, in: 7th International Symposium on Utilization of High Strength High Performance Concrete, Washington DC, United States. 2005. 1 51-78.
[10] J. Piérard, B. Dooms, N. Cauberg. Evaluation of durability parameters of UHPC using accelerated lab tests, in: Proceedings of the 3rd International Symposium on UHPC and Nanotechnology for High Performance Construction Materials, Kassel, Germany. 2012. 371-376.
[11] T.(.M. Ahlborn, D.K. Harris, D.L. Misson, E.J. Peuse, Characterization of strength and durability of ultra-high-performance concrete under variable curing conditions, Transp. Res. Rec.: J. Transp. Res. Board 2251 2251 (1) (2011) 68–75.
[12] B. Graybeal, J. Tanesi, Durability of an ultrahigh-performance concrete, J. Mater. Civ. Eng. 19 (10) (2007) 848–854, https://doi.org/10.1061/(ASCE)0899-1561(2007)19:10(848).
[13] M. Alkaysi, S. El-Tawil, Z. Liu, W. Hansen, Effects of silica powder and cement type on durability of ultra high performance concrete (UHPC), Cem. Concr. Compos. 66 (2016) 47–56, https://doi.org/10.1016/j.cemconcomp.2015.11.005.
[14] S. Pyo, T. Koh, M. Tafesse, H.K. Kim, Chloride-induced corrosion of steel fiber near the surface of ultra-high performance concrete and its effect on flexural behavior with various thickness, Constr. Build. Mater. 224 (2019) 206–213, https://doi.org/10.1016/j.conbuildmat.2019.07.063.
[15] Q. Song, R. Yu, Z. Shui, S. Rao, X. Wang, M. Sun, C. Jiang, Steel fibre content and interconnection induced electrochemical corrosion of Ultra-High Performance Fibre Reinforced Concrete (UHPFRC), Cem. Concr. Compos. 94 (2018) 191–200, https://doi.org/10.1016/j.cemconcomp.2018.09.010.
[16] A.S. El-Dieb, Mechanical, durability and microstructural characteristics of ultra-high-strength self-compacting concrete incorporating steel fibers, Materials and Design 30 (10) (2009) 4286–4292, https://doi.org/10.1016/j.matdes.2009.04.024.
[17] Y.L. Voo, S.J. Foster, Characteristics of ultra-high performance 'ductile' concrete and its impact on sustainable construction, The IES Journal Part A: Civil & Structural Engineering 3 (3) (2010) 168–187, https://doi.org/10.1080/19373260.2010.492588.
[18] S. Abbas, A.M. Soliman, M.L. Nehdi, Exploring mechanical and durability properties of ultra-high performance concrete incorporating various steel fiber lengths and dosages, Constr. Build. Mater. 75 (2015) 429–441, https://doi.org/10.1016/j.conbuildmat.2014.11.017.
[19] M. Auroya, S. Poyeta, P. Le Bescopa, J.M. Torrentib, T. Charpentierc, M. Moskurac, X. Bourbon, Comparison between natural and accelerated carbonation (3% CO2): Impact on mineralogy, microstructure, water retention and cracking, Cem. Concr. Res. 109 (2018) 64–80, https://doi.org/10.1016/j. cemconres.2018.04.012.
[20] J.E. Ramón, J.M. Gandía-Romero, R. Bataller, M. Alcañiz, M. Valcuende, J. Soto, Potential step voltammetry: An approach to corrosion rate measurement of reinforcements in concrete, Cem. Concr. Compos. 110 (2020) 103590, https://doi.org/10.1016/j.cemconcomp.2020.103590.
[21] D.W.S. Ho, R.K. Lewis, Carbonation of concrete and its prediction, Cem. Concr. Res. 17 (3) (1987) 489–504, https://doi.org/10.1016/0008-8846(87)90012-3.
[22] V. Baroghel-Bouny, Conception des bétons pour une durée de vie donnée des ouvrages—Maîtrise de la durabilité vis-à-vis de la corrosion des armatures et de l'alcali-réaction—Etat de l'art et guide pour la mise en oeuvre d'une approche performantielle et prédictive sur la base d'indicateurs de durabilité, Scientific and Technical Report of the French Civil Engineering Association, AFGC, Bagneux, 2004.
[23] L. Nilsson, M.H. Ngo, O.E. Gjørv, in: High-performance repair materials for concrete structures in the port of Gothenburg, E & FN Spon, London, 1998, pp. 1193–1198.
[24] V.W.Y. Tam, X.F. Gao, C.M. Tam, Carbonation around near aggregate regions of old hardened concrete cement paste, Cem. Concr. Res. 35 (6) (2005) 1180–1186, https://doi.org/10.1016/j.cemconres.2004.07.042.
[25] M. Valcuende, C. Parra, E. Marco, A. Garrido, E. Martínez, J. Cánoves, Influence of limestone filler and viscosity-modifying admixture on the porous structure of self-compacting concrete, Constr. Build. Mater. 28 (1) (2012) 122–128, https://doi.org/10.1016/j.conbuildmat.2011.07.029.
[26] P. Garcés, M.A. Climent, E. Zornoza, Corrosión de armaduras en estructuras de hormigón armado, Ed. Editorial Club Universitario, Alicante, Spain, 2008.
[27] L. Bertolini, B. Elsener, P. Pedeferri, E. Radaelli, R. Polder, Corrosion of Steel in Concrete: Prevention, Diagnosis, Repair, second ed., Wiley-VCH, Germany, 2013.
[28] M.C. Alonso, M. Sanchez, Analysis of the variability of chloride threshold values in the literature, Materials and Corrosion 60 (8) (2009) 631–637, https://doi.org/10.1002/maco.200905296.
[29] U. Angst, B. Elsener, C.K. Larsen, Ø. Vennesland, Critical chloride content in reinforced concreted, a review, Cem. Concr. Res. 39 (2009) 1122e1138.
[30] COST 509. Corrosion and protection of metals in contact with concrete, Final report, in: Cox RN, Cigna R, Vennesland O, Valente T. Editors, European Commission, Directorate General Science, Research and Development, Brussels. 1997.
[31] R.R. Hussain, A. Alhozaimy, A. Al Negheimish, R. Al-Zaid, D.D.N. Singh. Mechanism of nucleation and growth of passive film on steel reinforcing bar at different durations of its exposure in concrete pore solution at nanoscale. ACI Mater J. 112(4). 2015. 523-534. https://doi.org/10.14359/51687662.
[32] L. Fan, W. Meng, L.e. Teng, K.H. Khayat, Effect of steel fibers with galvanized coatings on corrosion of steel bars embedded in UHPC, Composites Part B 177 (2019) 107445, https://doi.org/10.1016/j.compositesb:2019.107445.
[33] C. Andrade, C. Alonso, J.A. Gonzalez. An initial effort to use de corrosion rate measurements for estimating rebar durability, Corrosion rates of steel in concrete. Ed. N. Berke, V. Chaker, D. Whiting. ASTM STP 1065, Philadelphia. 1990. 29-37.
[34] S. Pyo, M. Tafesse, H. Kim, H.K. Kim, Effect of chloride content on mechanical properties of ultra high performance concrete, Cem. Concr. Compos. 84 (2017) 175–187, https://doi.org/10.1016/j.cemconcomp.2017.09.006.